

Inflation deployed torus-shaped solar sail accelerated via thermal desorption of coating

Roman Ya. Kezerashvili^{1,2}, Olga L. Starinova³, Alexander S. Chekashov³, Dylan J. Slocki⁴

¹*New York City College of Technology, The City University of New York,
Brooklyn, NY 11201, USA*

²*The Graduate School and University Center, The City University of New York,
New York, NY 10016, USA*

³*Samara National Research University, Russian Federation, Samara, Russia*

⁴*State University of New York at Buffalo, Buffalo, NY 14228, USA*

(Dated: August 23, 2019)

A torus-shaped sail consists of a reflective membrane attached to an inflatable torus-shaped rim. The sail's deployment from its stowed configuration is initiated by introducing inflation pressure into the toroidal rim with an attached circular flat membrane coated by heat-sensitive materials that undergo thermal desorption (TD) from a solid to a gas phase. Our study of the deployment and acceleration of the sail is split into three steps: at a particular heliocentric distance a torus-shaped sail is deployed by a gas inflated into the toroidal rim and the membrane is kept flat by the pressure of the gas; under heating by solar radiation, the membrane coat undergoes TD and the sail is accelerated via TD of coating and solar radiation pressure (SRP); when TD ends, the sail utilizes thrust only from SRP. We study the stability of the torus-shaped sail and deflection and vibration of the flat membrane due to the acceleration by TD and SRP. The stability of the toroidal rim is addressed.

Keywords: Solar sail, thermal desorption, inflatable spacecraft vehicle, torus

I. INTRODUCTION

Electromagnetic radiation of the Sun is the abundant source of energy in space, it can provide spacecraft with a gentle yet persistent thrust for interplanetary and interstellar missions by means of a solar sail. Solar sail spacecraft offer an alternative to the traditional propulsion systems that must carry their fuel on the vehicle. A solar sail is a large sheet of low areal density material that captures or reflects the Sun electromagnetic flux as a means of acceleration [1–4]. The solar sail navigates by changing the orientation or reflectivity of the sails. These factors benefit performance since the spacecraft no longer needs to carry the mass of a propulsion system. This in turn benefits the acceleration of the solar sail. The initial launch of a solar sailing spacecraft is typically more affordable due to having a lighter weight. It would also not require refueling missions that can limit the longevity of the spacecraft. The proposals to use solar sails covers almost the whole spectrum of space missions, from the construction of a lunar base to an expedition to Mars, from scientific probes to mining exploitation of the asteroids, even implementations for deep space exploration and interstellar travel are considered.

Solar sails come in various types, typically being rigid flat squares with mechanical booms that keep the sail material in place. A few of these beams are under compressive loads with stay wires that keep the sail relatively flat. Canopy sails are similar in construction to parachute sails or pillow sails. They use the solar radiation pressure to remain open much like a parachute uses air. Canopy sails decrease the required mass and stiffness in relation to a decrease of performance. Less of the actual area is used for propulsion as a result of increased curvature. Many different systems have been previously considered for the sails opening. Each system was characterized by the presence of guide rollers, electromechanical actuation devices, or composite booms [5]. Most recently an alternative method for the solar sail self-deployment based on shape memory alloys was suggested [6, 7], where the authors use of shape memory alloys as mechanical actuators for solar sail self-deployment instead of heavy and bulky mechanical booms. However, in the actual deployment technology, the main limit is still the high weight of the system and the complexity of the deployment mechanism for solar sail surface.

The concept of using inflatable structures for spacecraft has been extensively discussed during the past six decades and dates back to the 1950's. The Echo balloons launched in the 1960s by NASA were some of the first inflatable to be utilized [8]. This was followed by the Inflatable Antenna Experiment around the middle of the 1990s [9]. Throughout the 1960s and early 1970s, NASA and industry teams were at

work developing inflatable space structures ranging from space suits to habitats [10]. Space inflatable composite structures offer great advantages over rigid structures due to being flexible and more compatible low volume storage for launch. Once these structures are inflated and deployed, they operated with similar principals to rigid structures to obtain comparable or greater performance. Inflatable structures are becoming more robust and durable following the advancement and development of flexible polymers and high strength fibers. This allows for increasingly smaller mass packed into a dense prelaunch storage, which further reduces costs [10]. Inflatable space structures have a simple deployment mechanism for large space structures besides being beneficial from their light-weight and small volume for launch. Inflatable structures, which have been the subject of renewed interest in recent years and investigated in detail in Refs. [11, 12], have characteristics that are particularly advantageous for a solar sail. First, they are extremely lightweight, which makes them an ideal match for use with low thrust solar sails, where sail weight is critical. The second obvious advantage is the ability to deploy in orbit and related space savings in the launch configuration. Therefore, inflatable structures possess special properties such as low weight, minimal stowage volume and high stretch-to-fold ratios that make them suitable for solar sails. In 1989 Jorg Strobl in Ref. [13] proposed a hydrogen inflated hollow disk-shaped sail with a molybdenum reflector. This hollow body solar sail concept was later applied to the design of an orbiting radio telescope [14]. Matloff [15] reinvestigated and revived the hollow-body solar sail an interstellar travel concept. Space-environment effects on beryllium hollow-body sails with hydrogen fill gas unfurled was investigated in details in Refs. [16, 17]. In Ref. [18] the concept of the solar sail with inflatable beams was suggested, which are kept pressurized after deployment, relieves all compressive stresses, allowing a very simple configuration and a straightforward deployment procedure. The solar sail with inflatable booms, that unfold to support the sail and control vanes at the corners was analyzed in Ref. [19]. The idea of the inflatable ring sail or the torus solar sail was presented in Ref. [20], where a circular sail with an inflatable outer ring was considered.

The acceleration of the solar sail by thermal desorption of a coating was proposed by Benford and Benford [21]. In this case the reflective area of the sail should be coated by the material that undergoes the thermal desorption when beam powered microwave pulse from the source located on the Earth or on an orbit is used for heating. The experimental study [22] demonstrated that desorption can attain high specific impulse if low mass molecules or atoms are blown out of a lattice of material at high temperature. However, the solar sail is naturally heated through the absorption of solar radiation. It was suggested to utilize the concept of thermal desorption to the solar sail that naturally gains temperature through the absorption of solar radiation at a particular point in a heliocentric orbit where the temperature of the solar sail corresponds to the temperature of thermal desorption of the coating material [23]. It is of particular interest to consider an inflatable torus-shaped solar sail as both propellant-less and propellant-based system. It is a propellant-based and a propellant-less system which create thrust by the sun-driven ejection of a flux of particles of non-zero rest mass due to the desorption of coating and solar radiation pressure, while it performs as a propellant-less conventional solar sail after the thermal desorption ends.

In this paper we consider the dynamics of a deployed torus-shaped sail, which can be unfurled using an inflatable torus-shaped rim structure. The torus-shaped sail consists of a thin reflective membrane attached to an inflatable torus-shaped rim. The sail's deployment from its stowed configuration is initiated by introducing inflation pressure into the toroidal rim with a round flat membrane coated by special heat-sensitive materials that undergo the transition from the solid state phase into the gas phase [21]. The membrane is kept open and flat by the distribution of the dynamic pressure of the gas in the toroidal rim. The deployment and acceleration of the solar sail could be split into three steps: in the first step, at a particular heliocentric distance the torus-shaped solar sail is deployed by the gas inflated into the toroidal structure and the membrane, which is coated with materials that undergo thermal desorption (TD) at a specific temperature, is extended to a final flat shape; in the second step, the membrane coat undergoes TD as a result of heating by solar radiation and the inflation deployed torus-shaped solar sail is accelerated via TD of coating [23] as well as by solar radiation pressure; in the third step, when the TD process ends, the sail utilizes thrust only from the Sun and escapes the Solar System through the conventional acceleration due to solar radiation pressure (SRP). We determine the required structural strength of the inflatable torus to support the flat surface of a circular membrane of a solar sail and study the deflection of the flat membrane due to accelerations initiated by TD and SRP using the equation of membrane. While the governing equation for a gas in an inflated torus is assumed to be the equation for an ideal gas. Within such approach we investigate the effects of both the enclosed gas pressure and structure stiffness on the mode shapes of the inflated torus and the stability of the torus-shaped solar sail. It is demonstrated that the effect of the enclosed gas must be considered in the dynamic analysis of

the inflatable torus with the membrane.

The paper is organized in the following way. In Sec. 2 the dynamics of a sail with thermal desorption of coating is considered. The solar sail configuration is described in Sec. 3. In particular, it is considered outer edge of a sail - a toroidal rim, and characteristics of a toroidal shell. In the next subsections we analyze the sail membrane deflection under the solar radiation pressure and the pressure induced by the thermal desorption of the coating material, as well as vibrations of the membrane is addressed, while in Subsec. 3.3 is analyzed the pressure of the gas which fills the toroidal rim required to unfurl the sail and provide a desired tensile strength. The effect of the electrostatic pressure for deployment of the sail is discussed in Subsec. 3.4. In Sec. 4 are given results of calculations and discussion. Conclusions follow in Sec. 5.

II. DYNAMICS OF A SAIL WITH THERMAL DESORPTION OF COATING

Thermal desorption produces thrust via releasing atoms at high speed from the surface of the coated sail and acts like a jet plate. This release is assumed to occur normal to the coating surface. Therefore, the coating mass varies and at any instant t it can be presented as $M_c(t) \equiv M_c = M_0 - m_0 t$, where M_0 is the total coating mass and $\frac{dM_c(t)}{dt} = -m_0$ is the rate of desorption. It is obvious that the total time of the acceleration due to the desorption is equal to the time of the desorption, and thus $t_D = \frac{M_0}{m_0}$. The coated unfolded sail is a moving object with variable mass due to coating material loss during the desorption period. At the end of the desorption process $t = t_D$, one has $M_c(t_D) = 0$, namely the coating mass is completely desorbed. The fact of the variation of mass during the desorption cannot be neglected and should be taken into consideration. Moreover, for the stability of the sail, it is important to have a symmetric coating mass distribution on the surface of the sail. The total instantaneous mass of the torus-shaped solar sail with the area A and areal mass of the membrane σ is $M(t) = \sigma A + M_t + M_P + M_c$, where M_t and M_P are the mass of the torus filled with the gas of mass M_g and mass of the payload, respectively. Since the total mass of the coated sail varies in time, the force on the sail can be written as

$$F = \frac{d}{dt} (M(t)v) = (\sigma A + M_t + M_P + M_c) \frac{dv}{dt} + \frac{dM_c}{dt} v. \quad (1)$$

However, in our case the solar sail utilizes thrust from the TD of coating and solar radiation pressure. The force due to the thermal desorption is $F = \frac{dM_c}{dt} v_{th}$, where v_{th} the thermal speed of desorpted atoms of the coating material. According to Maxwell's electromagnetic theory, solar electromagnetic radiation carries the energy and linear momentum and the radiation pressure exerted on a surface due to momentum transport by photons is $P_s = \frac{k}{r^2}$, and produces the resulting force $\frac{k}{r^2} A$, where A is the surface area facing the sun and $k = \frac{\eta L_s}{2\pi c}$. In the latter expression $L_s = 3.842 \times 10^{26}$ W is the solar luminosity, c is the speed of light and $0.5 \leq \eta \leq 1$. The case $\eta = 0.5$ corresponds to the total absorption of photons by the solar sail and $\eta = 1$ corresponds to total reflection. Therefore, the resultant force produced by the desorption and solar radiation pressure is

$$F = \frac{dM_c}{dt} v_{th} + \frac{k}{r^2} A. \quad (2)$$

By comparing equations (1) and (2) one obtains a differential equation for v :

$$\frac{dv}{dt} - G(t)v + G(t) \left(v_{th} - \frac{kA}{r^2 m_0} \right) = 0. \quad (3)$$

In Eq. (3) we introduce the time-dependent coefficient $G(t)$ defined as

$$G(t) = \frac{m_0}{(\sigma A + M_t + M_P + M_0 - m_0 t)} \quad (4)$$

by considering that $M_c = M_0 - m_0 t$ and $\frac{dM_c}{dt} = -m_0$.

We solve the first order differential equation (3) with time-dependent coefficient $G(t)$ assuming that when the torus-shaped sail is deployed at the perihelion of the heliocentric orbit, where the mechanism of the thermal desorption is turned on at $t = 0$, the sail's velocity is v_p , *i.e.* $v(0) = v_p$ is the sail's velocity at the perihelion of the heliocentric orbit. The corresponding solution of Eq. (3) is

$$v(t) = G(t) \left[\frac{v_p(\sigma A + M_t + M_P + M_0)}{m_0} - \left(v_{th} - \frac{kA}{r^2 m_0} \right) t \right]. \quad (5)$$

In Eq. (5) v_{th} is the thermal speed of the desorbed atoms, which depends on the temperature T of the membrane and the mass m of the atoms and is defined by the Maxwell speed distribution as

$$v_{th} = \sqrt{\frac{8k_B T}{\pi m}}, \quad (6)$$

where $k_B = 1.38 \times 10^{-23} \text{ J}\cdot\text{K}^{-1}$ is the Boltzmann constant. Therefore, the velocity of the sail is determined by the initial velocity of the sail at the perihelion v_p , and depends on the rate of desorption m_0 , the thermal speed v_{th} of the desorbed atoms, as well as on the solar radiation pressure. By the end of the acceleration due to desorption at $t_D = \frac{M_0}{m_0}$ the sail will gain the maximum velocity

$$v_{\max} = v_p + \left(v_p - v_{th} + \frac{kA}{r^2 m_0} \right) \frac{M_0}{\sigma A + M_t + M_P}. \quad (7)$$

Eq. (7) shows that the maximal velocity of the sail is determined by the initial velocity of the sail v_p at the perihelion of the heliocentric orbit, and ratio of coating mass M_0 to mass of the sailcraft $\sigma A + M_t + M_P$ excluding the coating mass. With this velocity, the sail continues to accelerate due to the solar radiation at a lower rate but for a longer time interval. The corresponding description of the sail acceleration due to the solar radiation is well known and can be omitted here.

For the sake of simplicity in calculations of the maximum velocity using Eq. (3), one can neglect the contribution of the term $\frac{kA}{r^2 m_0}$ related to the force due to solar radiation during the desorption phase because the acceleration due to the thermal desorption is considered to be a rapid enough process to allow this simplification. Of course, acceleration due to solar radiation pressure increases the sail's velocity when thermal desorption is occurring over close approach, but its contribution is not significant because the desorption phase is so short, only a few thousand seconds. The corresponding analytical expressions for the velocity of the sail and the reasonability of this approximation is discussed in details in Refs. [24–26]. Also one should mention that the high reflectivity you want in a good solar sail is diametrically opposed to the high absorptivity you want in a coating material that's going to evaporate off.

III. SOLAR SAIL CONFIGURATION

Below we consider the main elements of the torus-shaped solar sail: the toroidal rim, which deploys the solar sail, the sail's membrane, and the required pressure of the gas within the toroidal shell.

A. Outer edge of a sail: a toroidal rim

A toroidal rim is a key component and basic structural element functioning to carry the load imposed by the inflation pressure as well as take up the tensile forces created by the stretched membrane at the inner edge and provides structural support to the sail. Here we consider a structural static behavior of an inflated toroidal rim following Ref. [27]. We assume large aspect ratio, the thickness of the torus shell is negligible compared to the radii of curvature, an inflated gas affects moderately to out-plane loading condition with more peaks compared to that of the in-plane loading condition and any change in length from deformation is insignificant and can be neglected.

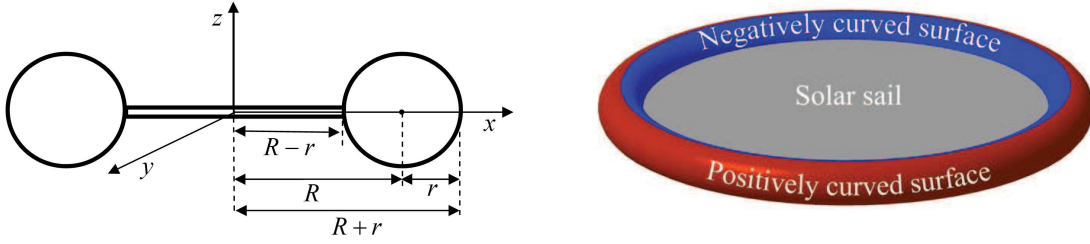


FIG. 1: (Color online) Torus-shaped solar sail and its geometric characteristics.

In the left panel in Fig. 1 the torus with circular cross section that is generated by revolving the circle $(x - R)^2 + z^2 = r^2$ of radius r in the xz - plane about the z axis at the distance R from the center of the circle is shown. For a ring torus with a large aspect ratio we have $R \gg r$. An implicit equation in Cartesian coordinates for a torus azimuthally symmetric about the z -axis is

$$(R - \sqrt{x^2 + y^2})^2 + z^2 = r^2, \quad (8)$$

where R is the distance from the center of the tube to the center of the torus and r is the radius of the tube.

It is convenient to use toroidal and poloidal coordinates. The polar coordinate (r, ϕ) at each cross section and circumferential (toroidal) coordinate θ around the toroidal ring are chosen to describe the geometric variation in the torus. The toroidal coordinate with an origin at the center of the torus is used to describe those quantities along the direction normal to the cross section. The three coordinate set r, ϕ, θ of curved coordinate system are orthogonal to each other. Then the toroidal and poloidal coordinate system relates to standard Cartesian coordinates with basic toroidal geometry are equated as

$$\begin{aligned} x &= (R + r \cos \phi) \cos \theta, \\ y &= (R + r \cos \phi) \sin \theta, \\ z &= r \sin \phi. \end{aligned} \quad (9)$$

Our special interest is on the surface area of the torus. The total surface area of the torus can be considered as a sum of the outer and inner surfaces (right panel in Fig. 1). The torus have two curvatures in two principal direction causes coupling between bending and stretching actions of a membrane. The outer surface is a positively curved in a contrast of the inner surface, which is negatively curved. The surface is positively curved, if a tangent plane placed on any point on the outer surface, all the points on the surface of the torus will be curving away from it on one side of the plane only, whereas a negatively curved surface a tangent plane located on any point on the inner surface, results of points on the torus that curve away on both sides of the plane. Our interest is to find how much larger is the outer surface than the inner one. Let us find surface area of both positively and negatively curved surface areas. If the measure of the length is $s = r\phi$, thus $ds = r d\phi$, where $\phi \in [\frac{\pi}{2}, \frac{\pi}{2}]$. Therefore, the outer surface area of the torus is

$$A_{out} = \int_{-\frac{\pi}{2}}^{\frac{\pi}{2}} 2\pi (R + x) ds = \int_{-\frac{\pi}{2}}^{\frac{\pi}{2}} 2\pi (R + r \cos \phi) r d\phi = 2\pi^2 Rr + 4\pi r^2. \quad (10)$$

For the area of negatively curved surface one obtains

$$A_{in} = \int_{-\frac{\pi}{2}}^{\frac{\pi}{2}} 2\pi (R - x) ds = \int_{-\frac{\pi}{2}}^{\frac{\pi}{2}} 2\pi (R - r \cos \phi) r d\phi = 2\pi^2 Rr - 4\pi r^2. \quad (11)$$

Therefore, the positively curved surface is larger than the inner surface as much as

$$\Delta A = 8\pi r^2, \quad (12)$$

while the surface area of the torus is

$$A = A_{out} + A_{in} = 4\pi^2 r R. \quad (13)$$

The interior volume of the torus can be computed from Pappus' centroid theorem and is given by

$$V = 2\pi^2 r^2 R. \quad (14)$$

The volume of the filled gas is determined by the interior volume of the torus and given by (14).

Let us determine the mass of the sail. We assume that the surface of the torus is made from a material with density ρ_t and the density of the material of the membrane, which has the area $A = 4(R - r)^2$, is ρ_m . If the thickness of the foil for the toroidal shell and membrane is the same and equals d , the mass of the sail is

$$M = \sigma A + M_t = 4\pi^2 \rho_t r R d + \pi \rho_m (R - r)^2 d + M_g, \quad (15)$$

where M_t is the mass of the toroidal shell filled with the gas of mass M_g .

B. Sail membrane

The sail surface is a circular membrane of radius $R - r$, which is considered as a disk of radius $R - r$, and height d centered at the origin, which will represent the "still" drum head shape under the tensile strength produced by toroidal rim. The boundary of the membrane is a circle of radius $R - r$ centered at the origin. Thus, the boundary is the inner part of the torus and represents the rigid frame to which the membrane is attached. In the equilibrium position the membrane is stretched and fixed along its entire boundary by the inflated toroidal rim in the xy -plane. The tension per unit length q caused by stretching the membrane is the same at all points and in all directions and does not change during the motion. The membrane is perfectly flexible and offers no resistance to bending. At any time the deflection of the membrane shape at a point is measured from this "still" membrane shape will be denoted by $\zeta(\rho)$, which can take both positive and negative values. Assuming that the shape in the loaded condition is shallow enough to linearize the problem, the equilibrium equation of the membrane in polar coordinates is [18]

$$\frac{d^2 \zeta(\rho)}{d\rho^2} + \frac{1}{r} \frac{d\zeta(\rho)}{d\rho} = -\frac{p}{q}, \quad (16)$$

where $\zeta(\rho)$ is the deflected configuration, q is the in-plane tensile force per unit length in the membrane and p is the pressure acting on the membrane. Eq. (16) has the analytical solution, yielding

$$\zeta(\rho) = \frac{p}{4q} [(R - r)^2 - \rho^2], \quad (17)$$

where $R - r$ is the outer radius of the sail.

During the thermal desorption acceleration, the membrane experiences both the solar radiation pressure and the pressure due to desorption of the coating material. The total pressure is

$$p = \frac{k}{r^2} + \frac{m_0 v_{th}}{A}, \quad (18)$$

where the first and second terms in (18) correspond to the pressure due to solar radiation and thermal desorption of coating material, respectively. This pressure depends on the heliocentric distance, the rate of

the desorption process and the thermal speed of the desorbed atoms. At the end of the desorption process only the solar radiation pressure acts on the membrane. The maximum deflection of the membrane is

$$\zeta_{\max} = \frac{1}{4q} \left(\frac{k}{r^2} + \frac{m_0 v_{th}}{A} \right). \quad (19)$$

From the other side when the desorption process ends the sail surface suddenly experiences less pressure which will cause the vibration of the surface of the sail. The mathematical equation that governs the vibration of the membrane is the wave equation with zero boundary conditions. The wave equation has been widely studied in the literature and is as follows:

$$\frac{\partial^2 u}{\partial t^2} = c_s^2 \left(\frac{\partial^2 u}{\partial x^2} + \frac{\partial^2 u}{\partial y^2} \right), \quad c_s^2 = \frac{q}{\sigma}, \quad (20)$$

where $u(x, y) = 0$ on the boundary of the membrane, σ is the mass per area of the solar sail, and $c_s = \sqrt{\frac{q}{\sigma}}$ is the sound speed. Eq. (20) is the two-dimensional wave equation, which is a second order partial differential equation. Due to the circular geometry of the membrane it is convenient to rewrite Eq. (20) using the cylindrical coordinates

$$\frac{\partial^2 u}{\partial t^2} = c_s^2 \left(\frac{\partial^2 u}{\partial \varrho^2} + \frac{1}{\varrho} \frac{\partial u}{\partial \varrho} + \frac{1}{\varrho^2} \frac{\partial^2 u}{\partial \theta^2} \right), \quad \text{for } 0 \leq \varrho < R - r, \text{ and } 0 \leq \theta \leq 2\pi \quad (21)$$

with the boundary condition $u(\varrho, \theta, t) = 0$ for $\varrho = R - r$, which means that the membrane is fixed along the boundary circle of the radius ρ in the xy -plane for all times $t \geq 0$. To determine solutions $u(\varrho, \theta, t)$ that are radially symmetric, we solve Eq. (21) following the three standard steps: i. using the method of separation of variables, we first determine solutions as $u(\varrho, \theta, t) = U(\varrho, \theta)V(t)$ and obtain two independent differential equations for $U(\varrho, \theta)$ and $V(t)$ functions; ii. from the solutions of those ordinary differential equations we determine solution (eigenfunctions) $U(\varrho, \theta)$ which satisfy the boundary condition $U(\varrho, \theta) = 0$ for $\varrho = R - r$ and find the corresponding eigenvalues. Then find the periodical solution $V(t)$ by solving the second differential equation; iii. we compose these solutions and obtain the radially symmetric solution $u(\varrho, t)$ that satisfy the conditions $u(\varrho, 0)$ and $\frac{\partial u(\varrho, t)}{\partial t}$ depend only on ρ . The corresponding solution is given in Appendix by Eq. (A5).

C. Torus filled with gas

Now let us determine the required structural strength of the inflatable torus to support the flat surface of a circular membrane of a solar sail. We assume that at equilibrium the pressure of the gas in the torus obeys to the isochoric process because it is confined in the given volume V of the torus which only slightly changes shape due to the applied gas pressure and the internal pressure remains normal to the surface. Seeking the simplicity let us describe the gas by the equation for the ideal gas

$$PV = \frac{M_g}{\mu} R_g T, \quad (22)$$

where M_g is the required mass of the gas not considering diffusion losses, μ and T is the molecular weight and temperature of the gas, and $R_g = 8.31 \text{ J}\cdot\text{K}^{-1}\text{mol}^{-1}$ is a universal gas constant. For the isochoric process one should maintain the pressure

$$P = \frac{M_g}{\mu} \frac{R_g T}{2\pi^2 r^2 R}. \quad (23)$$

As it follows from Eq. (23) the pressure of the confined gas is defined by its mass and temperature, and characteristic size of the torus: R and r . Using Eqs. (12) and (23) one can find the in-plane tensile force per unit length in the membrane produced by the inflatable torus filled with gas

$$q = \frac{\Delta AP}{2\pi(R-r)} = \frac{2}{\pi^2} \frac{M_g}{\mu} \frac{R_g T}{(R-r)R}. \quad (24)$$

The gas confined in the torus has a high temperature and therefore it can diffuse through the wall of the toroidal shell. Let us consider atomic diffusion - the process whereby the random thermally-activated gas atoms result in net transport through the toroidal foil shell. In case of hydrogen gas, hydrogen molecules, atoms and ions inside the torus can diffuse through the toroidal shell wall and escape, resulting in the sail slowly deflating. There is a concentration gradient in the toroidal shell wall, because the torus is filled initially with hydrogen, and there is no hydrogen on the outside. The equation for a flux of hydrogen through the toroidal shell foil is

$$\mathbf{j} = -D \left(\nabla C + C \frac{Q}{R_g T^2} \nabla T \right), \quad (25)$$

where Q is the heat transport, while D is the diffusivity, and C is the concentration which are measured in mol/m³ and m²/s, respectively. Below we consider hydrogen as a gas and beryllium as a material of the sail membrane and toroidal shell. In this case Eq. (25) contains two hydrogen-beryllium interaction parameters, the diffusivity D , which describes the hydrogen transport in a concentration gradient and the heat transport Q , which describes the hydrogen transport in a temperature gradient. Because the thickness of the toroidal shell wall is about a few tens of nanometers, the temperature gradient is negligibly small and in Eq. (25) to a very good approximation we can consider that $\nabla T = 0$. Therefore, the rate of transport of hydrogen is governed by the diffusivity and the concentration gradient and a diffusion flux can be determined by the Fick's first law [33] as

$$\mathbf{j} = -D \nabla C. \quad (26)$$

The diffusion coefficient D of the hydrogen through the material depends on the velocity of the diffusing particles, which in turn depends on the temperature, and the size of the particles and is defined by an Arrhenius equation $D = D_0 \exp\left(-\frac{E_D}{k_B T}\right)$, where D_0 is diffusion constant, E_D is the activation energy for the diffusion in electronvolts (eV) and $k_B = 1.38 \times 10^{-23} \text{ J} \cdot \text{K}^{-1} = 8.62 \times 10^{-5} \text{ eV/K}$ is the Boltzmann's constant. The hydrogen fill gas is in thermal equilibrium with the beryllium toroidal shell wall. Therefore, the gas temperature is equal to the temperature of the beryllium foil. In the best case scenario this temperature should be less than the beryllium melting temperature 1551 K.

For simplicity let us consider the diffusion flux perpendicular to the wall. Also the concentration of the hydrogen atoms decreases uniformly. Under these assumptions and due to very small thickness d of the beryllium toroidal shell wall as a good approximation we can replace the gradient of the concentration by the concentration difference $C_{out} - C_{in}$ over thickness d , where C_{out} and C_{in} are the concentration of hydrogen inside and outside of the beryllium toroidal shell. However, the outside concentration of the hydrogen $C_{out} = 0$ and in this case the Fick equation (26) can be rewritten as follows

$$j = D_0 e^{-\frac{E_D}{k_B T}} \frac{C_{in}}{d}. \quad (27)$$

Eq. (27) shows the dependence of the hydrogen diffusion flux on the temperature and thickness of the wall for the toroidal shell.

The total flux rate of the hydrogen through the toroidal shell area is

$$\frac{dM_g}{dt} = \oint \mathbf{j} \cdot \mathbf{n} dS, \quad (28)$$

where \mathbf{n} is the normal to the toroidal surface S . Using Eqs. (13) and (27) we can estimated the total mass flux rate as

$$\frac{dM_g}{dt} = 4\pi^2 R r D_0 e^{-\frac{E_D}{k_B T}} \frac{C_{in}}{d}. \quad (29)$$

D. Electrostatic pressure

Suppose that the toroidal shell surface is charged and the surface charge density is σ_c . The electric field just outside the charged torus is E and this field must be directed normal to the surface of the toroidal shell. Any parallel component would be shorted out by surface currents. Another way of saying this is that the surface of the toroidal shell, is an equipotential surface. The electric field inside of the hollow-body toroidal shell according to Gauss' law is zero, while at the surface of the toroidal shell it is $E = \frac{\sigma_c}{\epsilon_0}$. In the presence of an electric field, a surface charge on the toroidal shell will experience a force per unit area which is an outward electrostatic pressure. The electrostatic pressure can also be written as $P_e = \frac{\sigma_c}{2} E$, where E is the electric field immediately above the surface of the toroidal shell and is

$$P_e = \frac{\sigma_c^2}{2\epsilon_0}. \quad (30)$$

Note that the electrostatic pressure is equivalent to the energy density of the electric field immediately outside the torus. Electrostatic pressure acting on the toroidal surface produces the tensile force per unit length in the membrane as follows from Eqs. (12) and (30) is

$$q = \frac{\Delta A P_e}{2\pi(R-r)} = \frac{2}{\epsilon_0} \frac{\sigma_c^2 r^2}{(R-r)}. \quad (31)$$

The comparison of Eqs. (24) and (31) shows that the charge density $\sigma_c \sim 2 \times 10^{-3} \text{ C/m}^2$ will provide the same tensile force per unit length in the membrane as 0.3 – 0.5 kg of hydrogen.

The tensile strength of metals depends on the temperature. When temperature increases the tensile strength of materials usually decreases [31]. At room temperature the tensile strength of beryllium is 370 MPa, while at temperature 1100 K its tensile strength decreases to about 60 MPa [32]. The pressure of the gas inside of the toroidal shell when the temperature varies from 735 K ($r_p = 0.3 \text{ AU}$) to 1140 K ($r_p = 0.1 \text{ AU}$) is 0.12 MPa and 0.18 MPa, correspondingly. The same electrostatic pressure corresponds to the surface charge distribution on the toroidal shell $\sigma_c \sim 1.4 \times 10^{-3} \text{ C/m}^2$ and $\sigma_c \sim 1.8 \times 10^{-3} \text{ C/m}^2$, respectively. Hence, in our case the gas pressure or the electrostatic pressure does not exceeds the solar sail material's tensile strength, and therefore the surface of the toroidal shell will not fragment.

IV. RESULTS AND DISCUSSION

The objective of the present work is to propose a deployment and study dynamics of a sail, which can be unfurled using an inflatable torus-shaped rim structure. We consider the following scenario. Using a conventional spacecraft that carries the solar sails, the transfer occurs from Earth's orbit to Jupiter's orbit. After that a Jupiter flyby leads to the heliocentric orbit with the perihelion close to the Sun, where the temperature corresponds the temperature of thermal desorption of the coating material [34]. At this point the sail is deployed and thermal desorption becomes active. During a short period, the sail is accelerated by the thermal desorption and by solar radiation pressure. In our calculations we consider the following parameter of the torus-shaped solar sail: the radius of the toroidal rim and the torus tube of the sail is $R = 10 \text{ m}$ and $r = 0.2 \text{ m}$, respectively. The reflected membrane area $A = 301.72 \text{ m}^2$, while the thickness of the membrane and the toroidal shell $d = 40 \text{ nm}$. For this configuration the beryllium torus-shaped solar sail has the mass of membrane $\sigma A = 0.022 \text{ kg}$, mass of the toroidal rim $4\pi^2 \rho r R d = 0.006 \text{ kg}$, mass of the coating material $M_0 = 1.5 \text{ kg}$ with the rate of the desorption $m_0 = 1 \frac{\text{g}}{\text{s}}$, and we vary the molecular hydrogen fill gas from 0.2 to 0.5 kg. Depending on the perihelion approach the considered temperature range is 735 – 1140 K.

In Fig. 2 the results of the calculation of the deflection of the membrane due to the solar radiation pressure and both the thermal desorption of coating and solar radiation are shown. We perform calculations for different masses of the molecular hydrogen fill gas. The different mass of the confined gas lead to different pressure, which in turn changes the tensile strength applied to the membrane. The increase of the pressure leads to the increase of the tensile strength and, therefore, decreases the deflection of the

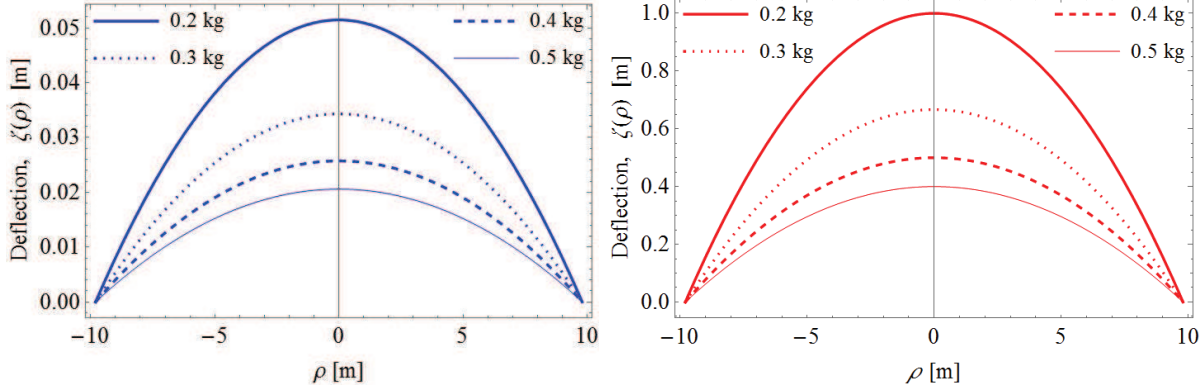


FIG. 2: Deflection of the membrane due to solar radiation (left panel) and thermal desorption (right panel).

membrane. Under the solar radiation the membrane experiences only a few cm deflection and maximum deflection from the flat position is varies from 0.08% to 0.3%. The deflection due to the both the thermal desorption and solar radiation is significantly larger. However, the maximum deflections for the different pressure of hydrogen gas is within a few percents only: 1.8% – 5%. In both cases the maximum deflection of the membrane inversely proportional to the mass of hydrogen fill gas.

We simulate the vibrations of the membrane under the following initial conditions: at the initial time, the membrane has the initial deviations ζ_{\max} and all its points have an initial velocity of 1 m/s. In modeling we consider the sum up the 20 terms of the series (A5), which is equivalent to the sum of 20 tones of membrane oscillations. Figures 3 and 4 show the simulation results. Figure 3 shows the shape of the deformed membrane surface for different instant of time. Figure 4 shows the process of membrane oscillation in 3D space.

Dynamics of an inflated torus is beyond the scope of present study and the vibrational behavior of inflated tori has been extensively discussed in the literature during the past six decades. Let us mentioned that analysis on inflatable torus has been done in many publications and a literature review [28] describes analytical as well as experimental works on the dynamic response of inflated torus. Most recent finite element analysis and effect of internal gas on modal analysis of an inflatable torus are given in Refs. [29, 30]

Let us consider the density of filled hydrogen gas. For the mass of gas 0.2 – 0.5 kg the density varies from $2.53 \times 10^{-5} \text{ kg/m}^3$ to $6.33 \times 10^{-5} \text{ kg/m}^3$. Thus, we are justifying that the hydrogen gas confined by the toroidal shell can be considered as an ideal gas. Using Eq. (29) we can determine the dependence the total flux rate of the hydrogen on the temperature of the material. Fig. 5 presents the results of our calculations for the dependence of the flux rate of the hydrogen on the temperature for the different values of the diffusion activation energy E_D and diffusion constant D_0 . The experimental value of the activation energy E_D and diffusion constant D_0 for the diffusion of beryllium depends on the purity of the

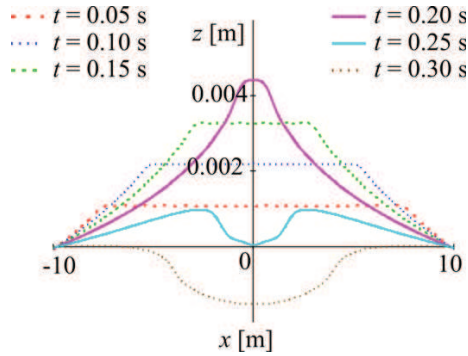


FIG. 3: (Color online) Dynamics of the vibrating membrane.

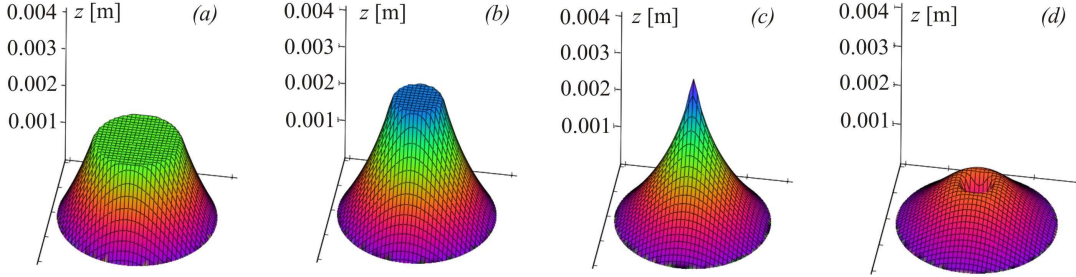


FIG. 4: (Color online) 3D dynamics of the vibrating membrane. (a) at $t = 0.1$ s; (b) $t = 0.15$ s; (c) $t = 0.20$ s; (d) $t = 0.25$ s.

beryllium material used in the experiments and varies from 0.16 eV to 0.19 eV and from 9×10^{-12} m²/s to 3×10^{-11} m²/s, respectively [35–37]. A general overview of these results shows that the diffused mass flux rate strongly depends on the temperature. When the temperature increases from 700 K to 1200 K, the flux rate increases by a factor of 5 and 2.5, when in calculations are used the diffusion activation energy and diffusion constant from Refs. [35] and [36], respectively. Hence, we can conclude that the results also demonstrated the strong dependence of the mass flux rate on the values of the diffusion activation energy and diffusion constant. The acceleration time of the torus-shaped solar sail nearby the Sun due to the thermal desorption is about 1500 s for the mass of the coating material 1.5 kg and desorption rate 1 g/s. Using these values we can estimate the performance time for the solar sail. From Fig. 5 it is easy to see that at the end of thermal desorption process only 85 g, which is about 28.5%, of the hydrogen filled gas will diffuse through the wall of the beryllium toroidal shell of the sail for the temperature regime up to 1200 K, when we used in our calculations the diffusion activation energy and diffusion constant from Ref. [35]. While only about 34 g (11.4%) of the hydrogen filled gas at the same temperature regime will diffuse through the wall of the toroidal shell, when we used the diffusion activation energy and diffusion constant from Ref. [36]. Therefore, we are on the safe side because the hydrogen pressure which corresponds to 0.2 kg of the gas still keeps the membrane flat with the maximum deflection of the membrane about 5 cm as this follows from the left panel of Fig. 2. If one will use 0.4 kg of hydrogen filled gas, the deflection of the membrane will not exceed about 3 cm and will gradually decrease with the increase of heliocentric distance due to the decrease of the solar radiation pressure.

In following preliminary analysis the planets and the Sun are considered point-like. In the heliocentric reference frame, assuming that Earth’s orbit is almost circular, the sail has to be transferred to an inner orbit closer to the Sun, in order to escape the Solar System. The transfer between these two coplanar circular orbits is different and depends on the proposed scenario. The results of calculations for a scenario for elliptical transfer plus slingshot plus thermal desorption acceleration are presented in Table 1. For each perihelion of the heliocentric escape orbit the corresponding speed at perihelion before

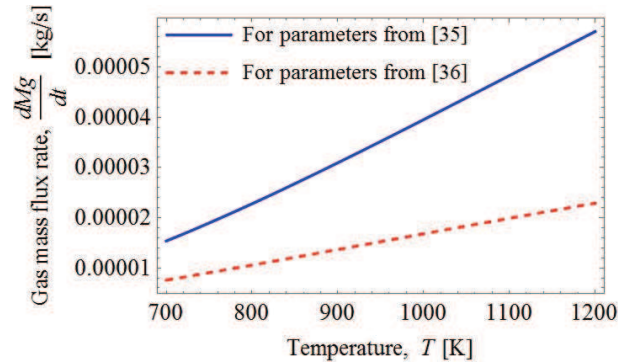


FIG. 5: (Color online) Temperature dependence of hydrogen flux rate through the toroidal beryllium shell. Results of calculation are given for the different diffusion activation energy E_D and diffusion constant D_0 .

TABLE I: Scenario for elliptical transfer plus slingshot plus thermal desorption acceleration. For each perihelion of the heliocentric escape orbit are presented the corresponding speed at perihelion before desorption v_p , the maximum speed v_{\max} after desorption, the eccentricity of the hyperbolic heliocentric orbit, temperature at the perihelion, cruise speed v_c with out solar radiation pressure, v_{sc} cruise speed including the solar radiation pressure, and distance D_y covered by a solar sail per year without TD and D_{s_y} is a distance covered by a solar sail per year with TD. Calculations are performed for the coating mass $M_c = 1.5$ kg, desorption rate $m_0 = 1$ g/s and mass of payload $M_P = 1.5$ kg.

Characteristics of the mission				
r_p	AU	0.3	0.2	0.1
v_p	km/s	73.24	91.23	129.11
T	K	735	864	1140
v_{\max}	km/s	133.23	166.20	235.35
e	–	1.01	2.12	5.26
v_c	km/s	110.33	138.2	194.09
v_{sc}	km/s	120.29	146.90	202.49
D_y	AU/year	23.21	29.08	41.05
D_{s_y}	AU/year	25.31	30.91	42.52

desorption v_p , the maximum speed v_{\max} after desorption, the eccentricity of the hyperbolic heliocentric orbit, temperature at the perihelion, cruise speed v_c and distance D_y covered by a solar sail per year are presented. Calculations are performed for the coating mass $M_c = 1.5$ kg, desorption rate $m_0 = 1$ g/s and mass of payload $M_P = 1.5$ kg. The eccentricity of the hyperbolic heliocentric orbit after the acceleration due to desorption ends is estimated as $e = v_{\max}^2 \frac{r_p}{\mu}$, where $\mu = 1.327 \times 10^{20} \text{ m}^3\text{s}^{-2}$ is the Sun’s gravitational parameter.

V. CONCLUSIONS

The advantage of inflation deployed torus-shaped solar sail accelerated via thermal desorption is clearly evident. The present study reveals that the inflation deployed torus-shaped solar sail accelerated via thermal desorption of coating results in high post-perihelion heliocentric solar sail velocities. With the speed 20–40 AU/year, post-perihelion travel times to the vicinity of Kuiper Belt Objects (KBO) will be less than 1 – 3 years, while the the Sun’s gravity focus at 547 AU can be reached in 13 – 25 years. We present the calculations for the Jupiter slingshot scenario but this would not make the Jupiter flyby a critical piece of the concept. Getting to perihelion can be accomplished a number of ways. The suggested configuration of the torus-shaped solar sail fits the cube-scale size configurations. Recent research reveals that much smaller sails could be incorporated with highly miniaturized chip-scale spacecraft. It is quite possible that a single dedicated interplanetary “bus” could deploy many cube-scale sails at perihelion. Sequential deployment of a fleet of solar sails could be timed to allow exploration of many small KBOs from a single launch. The natural continuation of this work can be extended in the following directions: i. detailed research on materials for thermal desorption at temperature suitable for solar sailing; ii. consideration of the Sun as an extended source of radiation; iii. study the influence of solar sail surface oscillations on the motion of a spacecraft performing an interplanetary flight.

Appendix A: Vibration of the membrane

Let us consider axisymmetric vibrations of the membrane. This means that the deviations of any point of the membrane depends only on the distance to the center of the membrane. Thus, we determine solutions $u(\varrho, t)$ that are radially symmetric. Based on this assumption and following Ref. [38], there is no angle dependence and Eq. (21) becomes simpler and takes the following form:

$$\frac{\partial^2 u}{\partial t^2} = c_s^2 \left(\frac{\partial^2 u}{\partial \varrho^2} + \frac{1}{\varrho} \frac{\partial u}{\partial \varrho} \right), \quad (\text{A1})$$

$$u(R-r, t) = 0 \text{ and for all } t \geq 0, \quad (\text{A2})$$

$$u(R-r, 0) = f(\varrho), \quad \frac{\partial}{\partial t} u(R-r, 0) = F(\varrho) \quad (\text{A3})$$

The conditions (A2)-(A3) in Eq. (A1) means that the membrane is fixed along the boundary circle $\varrho = R - r$ and the initial deflection $f(\varrho)$ and the initial velocity $F(\varrho)$ depend only on ϱ , not on θ , so that we can expect radially symmetric solutions $u(\varrho, t)$. The eigenfunctions $u_k(\varrho, t)$, obtained by solving equation (A1), have the form

$$u_k(\varrho, t) = [a_k \cos(\lambda_k ct) + b_k \sin(\lambda_k ct)] J_0(\lambda_k \varrho), \quad (\text{A4})$$

where $J_0(\lambda_k \varrho)$ are Bessel functions of zero order, $\lambda_k = \frac{\mu_k}{R-r}$ eigenvalues of the problem and μ_k are the roots of the zero-order Bessel function: $J_0(\lambda_k(R-r)) = 0$. The vibration of the membrane corresponding to $u_k(\varrho, t)$ is called the k th normal mode. One can obtain the solution of Eq. (A1) that satisfies the initial conditions by considering the series

$$u(\varrho, t) = \sum_{k=1}^n [a_k \cos(\lambda_k ct) + b_k \sin(\lambda_k ct)] J_0(\lambda_k \varrho), \quad (\text{A5})$$

where a_k and b_k must be the Fourier-Bessel series

$$a_k = \frac{2}{J_1(\mu_k)^2} \int_0^1 x J_0(\lambda_k x) f[(R-r)x] dx, \quad (\text{A6})$$

$$b_k = \frac{2(R-r)}{c^2 \mu_k J_1(\mu_k)^2} \int_0^1 x J_0(\lambda_k x) F[(R-r)x] dx, \quad (\text{A7})$$

where $x = \frac{\varrho}{R-r}$. The latter expressions are obtained from the condition for the fulfillment of boundary conditions.

-
- [1] E. N. Polyakhova, Kosmicheskii Polet s Solnechnim Parusom (Space Solar Sailing) (*in Russian*) Moscow, Nauka, 1986.
 - [2] C. R. McInnes, Solar Sailing - Technology, Dynamics and Mission Applications. Springer, Praxis Publishing, Chichester, 1999.
 - [3] G. L. Matloff, Deep Space Probes: To the Outer Solar System and Beyond. Springer/Praxis Books, 2005.
 - [4] G. Vulpetti, L. Johnson, G. L. Matloff, Solar Sails - A Novel Approach to Interplanetary Travel. Copernicus Books, 2008.
 - [5] J. M. Fernandez, V. J. Lappas, A. J. Daton-Lovett, Completely stripped solar sail concept using bi-stable reeled composite booms. Acta Astronautica **69**, 78–85 (2011).
 - [6] A. Boschetto, L. Bottini, G. Costanza, and M. E. Tata, Shape memory activated self-deployable solar sails: small-scale prototypes manufacturing and planarity analysis by 3D laser scanner, Actuators **8**, 38 (2019).
 - [7] A. Boschetto, L. Bottini, G. Costanza, and M. E. Tata, A novel self-deployable solar sail system activated by shape memory alloys, Aerospace **6**, 78 (2019).
 - [8] G. F. Pezditz, Erectable space structures-ECHO Satellites, NASA N62-12545, 1962.
 - [9] R. E. Freeland, G. D. Bilyeu, G. R. Veal, M. D. Steiner, and D. E. Carson, Large Inflatable Deployable Antenna Flight Experiment Results, Acta Astronautica, **41**, 267-277 (1997).
 - [10] D. Cadogan, J. Stein, and M. Grahne, Inflatable composite habitat structures for lunar and mars exploration, Acta Astronautica, **44**, 399–406 (1999).
 - [11] L. M. Leigh and M. L. Tinker, Dynamic characterization of an inflatable concentrator for solar thermal propulsion, J. Spacecraft and Rocket, **40**, 24–27 (2003).

- [12] K. B. Smalley, M. L. Tinker, and W. S. Taylor, Structural modeling of a five-meter thin-film inflatable antenna/concentrator, *J. Spacecraft and Rocket*, **40**, 27–29 (2003).
- [13] J. Strobl, The hollow-body solar sail, *JBIS*, **42**, 515–520 (1989).
- [14] J. Strobl, The hollow-body solar sail as a transporter of a Radio Telescope, *JBIS* **47**, 67–70 (1994).
- [15] G. L. Matloff, The beryllium hollow-body solar sail and interstellar travel, *JBIS* **59** 349–354 (2006).
- [16] R. Ya. Kezerashvili and G. L. Matloff, Solar radiation and the beryllium hollow-body sail: 1. The ionization and disintegration effects, *JBIS* **60**, 169–179 (2007).
- [17] R. Ya. Kezerashvili and G. L. Matloff, Solar radiation and the beryllium hollow-body sail: 2. Diffusion, recombination and erosion processes, *JBIS* **61** 47–57 (2008).
- [18] G. Genta and E. Brusa, The parachute sail with hydrostatic beam: a new concept for solar sailing. *Acta Astronautica* **44**, 133–140 (1999).
- [19] M. B. Quadrelli and J. West, Sensitivity studies of the deployment of a square inflatable solar sail with vanes, *Acta Astronautica* **65**, 1007–1027 (2009).
- [20] D. Hayn, The orbital torus solar sail vehicle (ORTOSS: Orbitaler Torus Sonnensegler), *Luft und Raumfahrt*, **11**, 34–36 (1990).
- [21] G. Benford and J. Benford, Acceleration of sails by thermal desorption of coatings, *Acta Astronautica* **56**, 593–599 (2005).
- [22] G. Benford and J. Benford, Desorption assisted sun diver missions. *AIP Conf. Proc.* **608**, 462–469 (2002).
- [23] R. Ya. Kezerashvili, *Acta Astronautica* **117**, 231–237 (2015).
- [24] E. Ancona and R. Ya. Kezerashvili, Orbital dynamics of a solar sail accelerated by thermal desorption of coatings, arXiv:1609.03131(2016) [physics.space-ph]; IAC 67, Guadalajara, Mexico, 2016, Paper ID: 32480.
- [25] E. Ancona and R. Ya. Kezerashvili, Extrasolar space exploration by a solar sail accelerated via thermal desorption of coating, *Advances Space Research* **63**, 2021–2034 (2019).
- [26] E. Ancona, R. Ya. Kezerashvili, and G. L. Matloff, Exploring the Kuiper Belt with sun-diving solar sails, *Acta Astronautica* **160**, 601–605 (2019).
- [27] H. Kraus, *Thin Elastic Shells*. Wiley, New York 1967.
- [28] E. Ruggiero, G. T. Bonnema, D. J. Inman, Application of SISO and MIMO modal analysis techniques on a membrane mirror satellites. In: *Proc. of 2003 ASME Int. Mech. Eng. Cong. and Exp.*, Aerospace Division, Washington, DC, November 2003, pp. 63–69, 2003.
- [29] S. C. Gajbhiye, S. H. Upadhyay, and S. P. Harsha, Finite element analysis of an inflatable torus considering air mass structural element, *Advances Space Research* **53**, 163–173 (2014).
- [30] F. Liu and W. He Effect of internal gas on modal analysis of space-inflatable structure, *J. Spacecraft Rockets*, **52**, 1258–1262 (2015).
- [31] T. Suzuki, I. Yonenaga and H. O. K. Kirchner, Yield strength of diamond, *Phys. Rev. Lett.* **75**, 3470 – 3472 (1995).
- [32] H. E. Boyer and T. L. Gall, Editors, “*Metals Handbook*”, American Society of Metals, Metals Park, OH, 1985.
- [33] A. Fick, *Phil. Mag.*, **10**, 30 (1855).
- [34] E. Ancona and R. Ya. Kezerashvili, Temperature restrictions for materials used in aerospace industry for the near-Sun orbits, *Acta Astronautica* **140** (2017) 565–569.
- [35] P. M. S. Jones and R. Gibson, Hydrogen in beryllium, *J. Nucl. Mater.* **21**, 353–354, 1967.
- [36] I. L. Tazhibaeva, V. P. Shestakov, E. V. Chikhray et al., *Proc. 18th Symp. Fus. Technol.*, 22–26 August, Karlsruhe, Fus. Technol. p.427, 1994.
- [37] R. A. Causey, Hydrogen Isotope retention and recycling in fusion reactor plasma-facing components, *J. Nucl. Mater.* **300**, 91–117 (2002).
- [38] A. S. Chekashov, O. L. Starinova, B. Alipova, I. V. Gorbunova, Modeling of solar sail surface oscillations during interplanetary flight, *J. Physics: Conf. Ser.* **1096**, 012064 (2018).